UC Riverside

UC Riverside Previously Published Works

Title

Transformative piezoelectric enhancement of P(VDF-TrFE) synergistically driven by nanoscale dimensional reduction and thermal treatment

Authors

Ico, G
Myung, A
Kim, BS
et al.

Peer reviewed

Nanoscale

Accepted Manuscript

Volume 8 | Number 1 | 7 January 2016 | Pages 1–660

Nanoscale

www.rsc.org/nanoscale

ISSN 2040-3364

PAPER
Qian Wang et al
TiC₂: a new two-dimensional sheet beyond MXenes

ROYAL SOCIETY OF CHEMISTRY

rsc.li/nanoscale

Transformative Piezoelectric Enhancement of P(VDF-TrFE) Synergistically Driven by Nanoscale Dimensional Reduction and Thermal Treatment[†]

G. Ico,[a] A. Myung,[a] B.S. Kim,[b] N.V. Myung[c] and J. Nam*[a]

a. Department of Bioengineering
University of California, Riverside
Riverside, CA 92521, USA

b. Korea Institute of Industrial Technology (KITECH)
Incheon 406-840, Korea

c. Department of Chemical and Environmental Engineering
University of California, Riverside
Riverside, CA 92521, USA

* Corresponding author. Email: jnam@engr.ucr.edu

Abstract

Despite the significant potential of organic piezoelectric materials in the electro-mechanical or mechano-electrical applications that require light and flexible material properties, the intrinsically low piezoelectric performance as compared to traditional inorganic materials has limited their full utilization. In this study, we demonstrate that dimensional reduction of poly(vinylidene fluoride trifluoroethylene) (P(VDF-TrFE)) at the nanoscale by electrospinning, combined with an appropriate thermal treatment, induces a transformative enhancement in piezoelectric performance. Specifically, the piezoelectric coefficient (d_{33}) reached up to -108 pm V^{-1}, approaching that of inorganic counterparts. Electrospun mats composed of thermo-treated 30 nm nanofibers with a thickness of 15 μm produced consistent peak-to-peak voltage of 38.5 V and power output of 74.1 μW at a strain of 0.26% while sustaining energy production over 10k repeated actuations. The exceptional piezoelectric performance was realized by the enhancement of piezoelectric dipole alignment and the materialization of flexoelectricity, both from the synergistic effects of dimensional reduction and thermal treatment. Our findings suggest that dimensionally controlled and thermally treated electrospun P(VDF-TrFE) nanofibers provide an opportunity to exploit their flexibility and durability for mechanically challenging applications while matching the piezoelectric performance of brittle, inorganic piezoelectric materials.

Nanoscale Accepted Manuscript

Introduction

Applications of piezoelectric materials have grown in the broad fields of actuators, sensors, and more recently for miniaturized energy harvesting electronics (e.g., wearable devices).[1-3] The piezoelectric conversion of salvageable mechanical energy (e.g., bodily movements and ambient vibrations) provides a sustainable electric source. Although inorganic piezoelectric materials such as lead zirconate titanate (PZT) and barium titanate ($BaTiO_3$) exhibit excellent piezoelectric properties, their brittle nature limits the applicability and long-term stability in flexible devices and mechanically challenging applications.

In this regard, organic polyvinylidene fluoride (PVDF) and its derivatives including a conjugated form with trifluoroethylene, P(VDF-TrFE), have demonstrated promising properties for flexible piezo- and ferroelectric applications.[4-7] PVDF is semi-crystalline, a critical characteristic for its mechanical compliance, and consists of three main phases depending on the conformation of the fluorine atoms to one another.[8] The α-phase is energetically favorable and is composed of chains conformed in trans (T) and gauche (G) linkages (i.e., TGTG'), which does not exhibit a molecular net dipole charge. The electroactive phases of PVDF include the β-phase (TTTT) and γ-phase (T_3GT_3G') for which the chain exhibits a net dipole charge perpendicular to the chain *c-axis*. Local crystalline domains, composed of either of the electroactive phases, respond to an external mechanical or electrical stimulus to produce the piezoelectric response. Therefore, the main approaches to enhance the piezoelectric properties of PVDF have been by increasing the electroactive phase content via mechanical/electrical poling [9] and thermal treatment.[10] Alternative approaches include stabilization of the electroactive phases at room temperature by incorporation of phase stabilizers (e.g., TrFE), which modulates polymer chain organization via steric hindrance.[8, 11] With approximately an order of magnitude lower piezoelectric coefficient, however, the piezoelectric performance of organic-based materials even with such efforts do not compare to their inorganic counterparts.

Recent studies of inorganic piezoelectric materials have shown significant piezoelectric enhancement via dimensional reduction below 100 nm.[12] In regards to organic-based materials, we have previously shown that a decrease in the fiber diameter of P(VDF-TrFE) via electrospinning induced enhancement of the piezoelectric properties, primarily due to an increase in the electroactive phase content and Young's modulus of the

nanofibers.[13] Nevertheless, the piezoelectric coefficient of P(VDF-TrFE) has not reached comparable levels of those found in commonly used inorganic piezoelectric materials.

In this work, the electrospinning process of P(VDF-TrFE) was optimized via solution tuning to produce the smallest possible nanofibers with an average fiber diameter of approximately 30 nm. Combined with a thermal treatment, the dimensional reduction in the nanofibers unexpectedly resulted in the highest piezoelectric coefficient (d_{33}) from any pure organic piezoelectric material, to the best of our knowledge, at approximately -108 pm V^{-1}. This value approaches the magnitude of the piezoelectric coefficient in inorganic piezoelectric materials. We demonstrate that this transformative improvement in the piezoelectric properties of P(VDF-TrFE) is largely due to the combination of an enhancement of the polarized domain alignment and the materialization of flexoelectricity, only realized by synergistic interactions between dimensional reduction and thermal treatment.

Experimental

Electrospinning of P(VDF-TrFE) nanofibers

A systematic approach was utilized to optimize solution properties including viscosity, conductivity and surface tension, in order to synthesize P(VDF-TrFE) nanofibers with an average fiber diameter of approximately 30 nm (**Figure S1-S5, Table S1**). A solution containing 1.3 wt.% P(VDF-TrFE) (70/30 mol%) (Solvay Group, France) dissolved in a 50/50 volume ratio of N,N-dimethylformamide (DMF) (Fisher Scientific, Pittsburgh, PA) and tetrahydrofuran (THF) (Sigma-Aldrich, St. Louis, MO), supplemented with 1.5 wt.% pyridinium formate (PF) buffer (Sigma-Aldrich, St. Louis, MO) and 0.05 wt.% BYK-377 (BYK Additives and Instruments, Wesel Germany) to increase and decrease the solution conductivity and surface tension, respectively, was utilized. Alternatively, P(VDF-TrFE) nanofibers with an average diameter of 90 nm were synthesized from a 4.0 wt.% P(VDF-TrFE) solution dissolved in 60/40 volume ratio of DMF and acetone (Fisher Scientific, Pittsburgh, PA) supplemented with 1.5 wt.% PF buffer.[13] Each solution was separately electrospun under optimized conditions of electrospinning distance (20 cm), applied voltage (approx. -15 kV) and solution feed rate (0.5 ml hr^{-1}) at 23 °C and an absolute humidity of 7.6 g m^{-3}.

Morphological characterization and phase analysis of P(VDF-TrFE) nanofibers

The morphology of electrospun nanofibers was characterized by scanning electron microscopy (FEI NNS450, FEI Corp., Hillsboro, OR). Fourier transform infrared (FTIR) of the electrospun fibers was conducted in absorbance mode from 600 to 1600 cm^{-1} with an Equinox 55 FTIR spectrometer (Bruker Corp., Billercia, MA). Five independent samples per condition were utilized to determine an average value of electroactive phase content. X-ray diffraction (XRD) peaks from each condition were collected from 2θ of 10-50° using an Empyrean X-ray diffractometer (PANalytical, Almelo, the Netherlands), and their patterns were analyzed to determine degree of crystallinity. Lattice constants were also determined from the XRD patterns. The combination of FTIR and XRD data was utilized to calculate the overall electroactive phase content.[13]

Piezoelectric coefficient measurement

To properly measure the piezoelectric coefficient, a standard periodically poled lithium niobate (PPLN) with a known piezoelectric coefficient was used to determine a correction factor for all subsequent measurements. Nanofibers were sparsely collected on a gold coated, thermal-oxide silicon substrate and subjected to single-point piezoresponse force microscopy on individual fibers. A MFP-3D AFM (Asylum Research, Santa Barbara, CA) was first used in tapping imaging mode to locate an individual fiber. Subsequently, the AFM was switched to PFM mode where single point spectroscopy measurements were conducted on five separate points along the length of each fiber with a specific fiber diameter. Step voltages from -3 to +3 V was applied across the fiber via the AFM cantilever (AC240TM, Olympus) to the grounded substrate. Alternatively, the thin film structure was achieved by collecting a thin fiber mat of 30 nm average diameter fibers on the same substrate and thermo-treated at 135 °C, and subjected to PFM measurements. A value of d_{33} was calculated by,

$$d_{33} = \frac{A}{VQ} f ,$$

where A is the amplitude response of the nanofiber in response to an applied voltage (V), Q is the quality factor of the AFM cantilever, and f is the correctional factor taken from the PPLN standard.

Electric output measurements

Nanofibrous mats of approximately 15 µm thickness were utilized for electric output measurements using a vibrational system modified from our previous report.[13] Briefly, the samples were cut to a rectangle with a size of 47x12 mm^2 and assembled into a cantilever using brass substrates (51x16 mm^2) (**Figure S6**). Since electrospinning process inherently induces mechanical stretching and electric field exposure to form fibers, the poling direction of piezoelectric materials has been shown to be perpendicular to the plane of the substrate.[13-16]. Therefore, the piezoelectric polarization direction of the nanofiber mats is perpendicular to the electrodes in the device. A proof mass of 2.3 g was placed at the end of the clamped cantilever to induce a bending strain under vibration. Voltage was measured utilizing an oscilloscope (Pico Technology, St Neots, United Kingdom) and power was calculated by utilizing the internal resistance of the oscilloscope (10 MΩ).

Alternatively, the same cantilever design was utilized in a custom-made strain cycler to demonstrate the durability of the flexible P(VDF-TrFE) after long-term strain exposure. Briefly, a 120 rpm gear motor was used as the driving force for an eccentric sheave that converts rotary to a linear reciprocating motion on a beam affixed to a ball bearing rail. The sample was driven for approximately 85 minutes to cycle the sample at 2 Hz for 10,000 cycles (**Movie S1**).

In addition, utilizing the same cantilever setup, the sample was fixed to a fitness armband to demonstrate the practical application of turning on low power wearable devices. The electrical leads from the cantilever was connected to a full-bridge rectifier to convert the AC voltage signal generated from the P(VDF-TrFE) to a DC output to power on and off multiple blue LEDs when the arm is repeatedly bent and extended (**Movie S2**).

Strain-gradient computational simulation

To determine the strain profile induced within an individual nanofiber under the compressive strain exerted by the AFM probe during piezoresponse measurements, a finite element analysis of structural mechanics by COMSOL Multiphysics was utilized. An arbitrary aspect ratio of 5:1 (length: diameter) was used to model

the nanofiber. The length was large enough to contain the AFM probe, which was modeled as a circular punch with a diameter of a 120 nm in order to encompass the 90 nm diameter nanofiber but small enough to reduce computational time. The cross section of the fiber was modeled as a core-sheath structure which has been shown to arise during electrospinning process due to non-uniform solvent evaporation, where the sheath thickness is independent and constant over a range fiber diameters.[17, 18] To assign the proper mechanical properties of the core and sheath for modelling, measured Young's Modulus data from individual P(VDF-TrFE) fibers having various fiber diameters were fitted with a non-linear regression of a rules of mixture model,[18]

$$E_f D_f^4 = E_c D_c^4 + E_s (D_f^4 - D_c^4),$$

where E_f is the measured elastic modulus of the fiber, E_c is the elastic modulus of the core, E_s is the elastic modulus of the sheath, D_f is the fiber diameter, and D_c is the diameter of the core. The core and sheath moduli were calculated to be approximately 1 and 6400 GPa, respectively, with a sheath thickness of approximately 8 nm. The AFM probe and underlying supporting substrate for the fiber were assigned with values of silicon within the built-in library. Fixed boundary constraints were applied to the AFM probe and substrate, and a fixed displacement of the AFM probe of -15% of the fiber diameter was used to impose compression on the fiber. The strain value was selected based on the average applied strain between the individual 30 and 90 nm diameter fibers during the actual PFM measurements at a fixed force. The third principle strain was observed for the analysis of the strain profile with respect to the diameter of the nanofiber and the differential of this strain with respect to the z-coordinate through the length of the cross-section was plotted for strain gradient analysis.

Results and Discussion

Synthesis of P(VDF-TrFE) nanofibers and their piezoelectric characterization

The piezoelectric properties of P(VDF-TrFE) nanofibers with an average fiber diameter of 90 nm (**Figure 1a**) or 30 nm (**Figure 1b**) were examined as-spun without thermal treatment (23 °C) or subsequently thermo-treated at 90 °C for 24 h. **Figures 1c and 1d** show that the thermal treatment did not alter the nanostructure of electrospun P(VDF-TrFE) for either size of 90 or 30 nm average fiber diameter, respectively. To investigate the effects of dimensional reduction and thermal treatment on the piezoelectric coefficient, single-

point piezoresponse force microscopy (PFM) measurements were conducted on individual fibers with approximately 30 or 90 nm fiber diameter. **Figure 1e** shows that the amplitude response of an individual 25 nm fiber is approximately 2-fold greater than that of an 85 nm nanofiber. Interestingly, the difference in the piezoelectric response between the two fiber sizes was further increased by the thermal treatment (**Figure 1f**). The exponential increase of d_{33} in response to reduction of the fiber diameter to a 30 nm range is shown in **Figure 1g**. More substantially, the thermal treatment combined with the dimensional reduction, induced a synergistic effect on the enhancement of d_{33}, especially below the fiber diameter of approximately 45 nm, reaching up to an average of -108 pm V^{-1} for a 28 nm nanofiber, the highest value reported for purely organic piezoelectric materials.

Piezoelectric performance of P(VDF-TrFE) nanofiber mats

To compare piezoelectric performance, 15 μm-thick mats composed of various electrospun P(VDF-TrFE) nanofibers with an average diameter of 30 nm, thermo-treated at 23 °C and 90 °C, or 90 nm at 23 °C were subjected to a controlled mechanical strain for energy generation (**Figure S6**). **Figure 2a** and **2b** show the peak-to-peak voltage and electric power generation as a function of applied strain, respectively, determined from the raw output voltage of the nanofiber mats under different applied strains (**Figure S7**). All measurements were conducted at open circuit, where the greatest electric output is observed (**Figure S8**). As expected, an increase in electric output is observed by simply reducing the fiber dimension from 90 to 30 nm due to the enhanced d_{33}. The thermal treatment of 30 nm nanofibers at 90 °C further increased the electric output, producing approximately 38.5 V and 74.1 μW at the maximum applied strain of 0.26%, an impressive enhancement of approximately 120% and 350% over those of untreated 90 nm nanofibers. Although a direct comparison to values in literature is not fully practical due to diverse testing platforms, the electric output reported here is at least an order of magnitude greater as compared to other PVDF piezoelectric based devices.[4, 19-21] Even with the limitation of applied strains, the observed 2.6 V$_{p-p}$ μm^{-1}, normalized to the thickness of the sample, at a strain of 0.26% outperforms the electric output values ranging from approximately 0.19 – 0.26 V$_{p-p}$ μm^{-1} in those studies.

Typical inorganic piezoelectric materials such as PZT and BaTiO$_3$ possess relatively low flexural yield strains of well below 0.2%.[22] This limits the application of inorganic piezoelectric materials typically to low displacements at high frequency ranges (hundreds of hertz).[23, 24] In contrast, we have demonstrated that P(VDF-TrFE) flexible nanofiber mats were able to operate at larger strains and at low frequencies (a few to tens of hertz). Additionally, the durability of electrospun P(VDF-TrFE) nanofibers was tested by subjecting the material to an actuation regimen repeated over 10,000 cycles at 2 Hz (**Movie S1**). Open-circuit voltage measured before and after the 10,000 cycles show that the sample maintained its piezoelectricity after the rigorous dynamic straining (**Figure 2c**). Considering the fact that the synthesized P(VDF-TrFE) nanofibers at 30 nm in this study exhibits a piezoelectric coefficient value similar to that of thin film BaTiO$_3$, we expect the organic piezoelectric material to be more efficient in its performance where inorganic-based materials would otherwise fail.[25-27] The exceptional flexibility with the potent piezoelectricity of electrospun P(VDF-TrFE) is demonstrated in an application for a wearable device in **Figure 2d (i).** A 15 μm-thick mat of 90 nm diameter fibers without the thermal treatment or 30 nm diameter fibers with the thermal treatment is attached to a fitness armband and connected to a full-bridge rectifier with a series of Super Bright blue LEDs. When the arm is in the extended static state the LEDs remains off (90 nm: **Figure 2d (ii)**, 30 nm: **Figure 2d (iii)**). A cycle between arm flexion and extension results in the LEDs turning on and off without the need for a capacitor (**Movie S2**). The mat composed of 90 nm diameter fibers was only able to turn on a maximum number of 3 LEDs (**Figure 2d (iv)**) while the mat composed of the thermo-treated 30 nm diameter fibers was able to light 10 LEDs (**Figure 2d (v)**). Therefore, our findings of the synergistic effects arising from dimensional reduction and thermal treatment on the piezoelectric performance of P(VDF-TrFE) nanofibers present promising potential applications for flexible thin-film-like devices.

Electroactive phase content quantification and its correlation to d_{33}

To understand the mechanism of such transformative enhancement on the piezoelectric performance of P(VDF-TrFE) nanofibers, synergistically by dimensional reduction and thermal treatment, the overall content of electroactive phases, the major determinant of d_{33}, was quantitatively determined by Fourier transform infrared

spectroscopy (FTIR) and X-ray diffraction (XRD). The FTIR spectra of P(VDF-TrFE) nanofibers having an

average diameter of 30 or 90 nm, both with and without the thermal treatment, are shown in **Figure 3a**, and were

utilized to calculate the electroactive phase content in the crystalline domains (**Figure 3b**). The electroactive

phase content of the as-spun P(VDF-TrFE) nanofibers (23 °C) increased as a function of fiber diameter. As

expected from the PFM results (**Figure 1**), the thermal treatment further increased the electroactive phase

content up to a maximum average of approximately 94% at the 30 nm average fiber diameter.

The XRD spectra of these fibers (**Figure 3c**) were subjected to peak deconvolution to quantify the

degree of crystallinity as a function of fiber diameter and thermal treatment (**Figure 3d**). As expected, an

increase in the degree of crystallinity was observed in the thermo-treated samples. The overall piezoelectric

response of P(VDF-TrFE) nanofibers are likely derived from and proportional to the overall electroactive phase

content, which was calculated from the product of electroactive phase in the crystalline and the degree of

crystallinity (**Figure 3e**). Surprisingly, the increase in electroactive phase content was not proportional to that in

the piezoelectric coefficient as 5% increase in electroactive phase content at the smallest fiber diameter by the

thermal treatment resulted in approximately 35% increase in d_{33}. **Figure 3f** shows an extrapolation of d_{33} with

respect to electroactive phase content of as-spun (23 °C) nanofibers, which predicts a d_{33} value of approximately

-60 pm V^{-1} at 100% electroactive phase content. However, the 25 nm nanofiber shows a deviation from this

prediction, reaching almost -60 pm V^{-1} at the electroactive phase content of only 71%. Such deviation was

further escalated by the thermal treatment, exhibiting a d_{33} of −108 pm V^{-1} for a 28 nm P(VDF-TrFE) nanofiber

at an overall electroactive phase content of 76%. The unexpected aberration of d_{33}, as much as approximately

35% increase from the prediction by electroactive phase content quantification, led us to investigate alternative

mechanisms responsible for such a substantial increase.

Piezoelectric dipole alignment

Electrospinning has been shown to induce polymer chain alignment by restricting the degree of freedom

in chain organization due to fiber elongation during the process, resulting in the high aspect ratio.[28, 29] It has been

also shown that the annealing of electrospun fibers further enhances chain alignment via thermo-induced chain

re-arrangement.[30, 31] To determine the effects of dimensional reduction and/or the thermal treatment on polymer chain/dipole alignment, hence piezoelectric performance, PFM phase imaging was conducted on P(VDF-TrFE) nanofibers with 30 or 90 nm average fiber diameter both as-spun (23 °C) and after the thermal treatment at 90 °C (**Figure 4**). Precise fiber location was determined from tapping imaging mode (3D images as shown), and the PFM phase imaging was conducted along the length of the fiber (inset) from which phase angle distribution profiles were determined. It should be noted that the pyramidal geometry of the AFM tip causes an imaging artifact in which the fiber appears wider than the actual fiber diameter (height) in the 3D image. Statistical analysis of the phase angle histograms from 3 independent nanofibers per condition shows that both dimensional reduction and the thermal treatment enhanced the alignment of piezoelectric domains in electrospun P(VDF-TrFE). The thermal treatment of 90 nm decreased the average phase angle from $15.3 \pm 9.9°$ (**Figure 4a**) to $2.9 \pm 2.3°$ (**Figure 4b**) while the dimensional reduction to 30 nm decreased it to $4.0 \pm 3.0°$ (**Figure 4c**). More significantly, the thermal treatment of 30 nm fibers further enhanced the piezoelectric phase alignment, resulting in an average phase angle of $2.7 \pm 2.2°$ (**Figure 4d**), partly explaining the observed substantial increase in d_{33} synergistically by dimensional reduction and thermal treatment.

Nanoscaling effects

To examine if nanostructuring of P(VDF-TrFE) via electrospinning also contributed to the substantially enhanced d_{33}, the nanofibers having an average fiber diameter of 30 nm were alternatively thermo-treated at 135 °C to destroy the nanostructure and subsequently subjected to piezoelectric characterization. **Figure 5a** depicts that this post-spinning thermal treatment abolished the nanofibrous structure, resulting in a rough film morphology. Albeit the loss of the nanofibrous structure, phase and crystallinity characterization by FTIR (**Figure S9a**) and XRD (**Figure S9b**) shows an increase in the total electroactive phase content (**Figure 5b** and **Figures S10a, S10b**). In spite of the high electroactive phase content, however, piezoelectric response dramatically decreased by the absence of the nanofibrous structure (**Figure 5c**). The d_{33} of the melted fiber mat after the thermal treatment at 135 °C exhibited a significantly reduced coefficient of -54 pm V^{-1} when compared to that of the 90 °C treated nanofibers at -108 pm V^{-1}. Interestingly, the d_{33} of an individual 30 nm nanofiber

after the thermal treatment at 135 °C, which retained its nanofiber structure, exhibited a similar value (-110 pm V^{-1}) to that of the individual nanofibers thermo-treated at 90 °C. Furthermore, when compared to the results presented in **Figure 2a**, destruction of the nanofibrous morphology by the thermal treatment at 135 °C resulted in a significant decrease in the open-circuit voltage production (**Figure S11**) of 38.5 V and 74.1 μW from the 90 °C sample down to 30.4 V and 46.2 μW at the highest strain (**Figure 5d**) comparable to the 23 °C sample whose d_{33} is also comparable to the melted mat. These results demonstrate that the nanostructuring of P(VDF-TrFE) is critical for the enhanced piezoelectric performance.

Possible mechanisms to account for the substantial increase in d_{33} from nanostructuring could be stemmed from piezoelectric crystal lattice change and/or flexoelectricity. Computational analysis of hexagonal GaN nanowires of varying diameter has shown that the absolute polarization and localized dipole moment are significantly affected by the dimension due to interatomic rearrangement with respect to wire diameter.[32] To examine if such lattice restructuring caused the transformative enhancement in the piezoelectric properties of electrospun P(VDF-TrFE), the unit cell lattice constants were calculated from the XRD data (**Figure 3C** and **S8b**). We note no significant change in the crystal lattice size for the 30 nm average fiber diameter samples thermo-treated at 23, 90 and 135 °C as well as nanofibrous mats of 90 nm average fiber diameter thermo-treated at 23 and 90 °C (**Table S1**). This may indicate insignificant atomic restructuring that affects piezoelectricity in P(VDF-TrFE) nanofibers, different from what was shown for the computationally determined GaN nanowire by dimensional reduction.

Another possible nanoscaling effect is the materialization of flexoelectricity by the dimensional reduction due to the close confinement of the surface and interior molecules/atoms.[33, 34] More specifically, the same surface stresses imparted on nanoscale materials composed of a few to tens of molecular layers induce greater strain gradients as compared to those of bulk materials.[35-37] These large strain gradients have been shown to impose a reconfiguration of the lattice structure and induce polarity in otherwise centrosymmetric materials which results in piezoelectric-like properties.[38] Such phenomenon, known as flexoelectricity, is also expected to further enhance piezoelectric responses in already piezoelectric materials by a similar mechanism,[35, 39] where the large strain gradient may further polarize the material likely in the non-electroactive phase under mechanical

loading.[40] In this regard, electrospinning creates a structure that may intensify flexoelectricity as it produces a thin sheath on the surface of the fibers due to non-uniform evaporation of solvent during the process.[17, 41] The thickness of the sheath, which exhibits a greater molecular density, hence higher mechanical modulus compared to the core,[18, 42] has been shown to remain constant independent of fiber diameter.[18] To determine the sheath thickness as well as the elastic moduli of the core and the sheath from P(VDF-TrFE) nanofibers, the modulus of P(VDF-TrFE) nanofibers with various fiber diameters was measured and fitted into a rule of mixture model (**Figure 6a**).[18] By utilizing the calculated parameters (sheath thickness: 8 nm, core modulus: 1 GPa, and sheath modulus: 6400 GPa), computational simulation results show that a compressive strain of 15% induces a greater radial strain gradient, perpendicular to the fiber length, in the smaller 30 nm fiber as compared to that of the 90 nm fiber (**Figure 6b**). Specifically, a significantly greater strain gradient in the 30 nm fiber near the fiber surface is observed likely due to the increasing contribution of the sheath as the overall fiber diameter decreases and the dramatically different moduli of the core and the sheath (**Figure 6c**). This indicates that dimensional reduction in combination with the native core-sheath structure of electrospun fibers, is critical to induce large strain gradients in the smaller nanofibers under mechanical loading, resulting in the realization of the flexoelectric phenomenon to augment piezoelectricity.

Conclusions

In summary, we investigated the effects of dimensional reduction and thermal treatment on the piezoelectric properties of electrospun P(VDF-TrFE). In particular, we report the highest d_{33} piezoelectric coefficient observed for a purely organic-based piezoelectric material. With dimensional reduction to approximately 30 nm in diameter of electrospun P(VDF-TrFE) nanofibers and post-spinning thermal treatment, we unexpectedly achieved a d_{33} value of -108 pm V^{-1}; an almost 60% increase as compared to as-spun nanofibers having a 3 times larger fiber diameter. Such transformative enhancement in piezoelectric performance was partly due to increased electroactive phase content, quantified by FT-IR and XRD. More significantly, we showed that the combination of dimensional reduction and thermal treatment synergistically induces the tightly distributed alignment of the electroactive domains and manifests the flexoelectric effect through greater strain gradients.

Overall, we demonstrate that proper synthesis of organic-based piezoelectric nanofibers at the nanoscale via optimized electrospinning and thermal treatment promotes a transformative enhancement of piezoelectric properties that are comparable to currently available inorganic materials while providing significantly superior mechanical resiliency.

Acknowledgements

References

1. W.-S. Jung, M.-J. Lee, M.-G. Kang, H. G. Moon, S.-J. Yoon, S.-H. Baek and C.-Y. Kang, *Nano Energy*, 2015, 13, 174-181.
2. M. Lee, C. Y. Chen, S. Wang, S. N. Cha, Y. J. Park, J. M. Kim, L. J. Chou and Z. L. Wang, *Advanced Materials*, 2012, 24, 1759-1764.
3. K. H. Mak, S. McWilliam and A. A. Popov, *Proceedings of the Institution of Mechanical Engineers, Part D: Journal of Automobile Engineering*, 2013, 227, 842-852.
4. V. Bhavanasi, V. Kumar, K. Parida, J. Wang and P. S. Lee, *ACS applied materials & interfaces*, 2015, 8, 521-529.
5. J. H. Lee, K. Y. Lee, M. K. Gupta, T. Y. Kim, D. Y. Lee, J. Oh, C. Ryu, W. J. Yoo, C. Y. Kang and S. J. Yoon, *Advanced Materials*, 2014, 26, 765-769.
6. R. I. Haque, R. Vié, M. Germainy, L. Valbin, P. Benaben and X. Boddaert, *Flexible and Printed Electronics*, 2015, 1, 015001.
7. Y. R. Wang, J. M. Zheng, G. Y. Ren, P. H. Zhang and C. Xu, *Smart Materials and Structures*, 2011, 20, 045009.
8. P. Martins, A. C. Lopes and S. Lanceros-Mendez, *Progress in polymer science*, 2014, 39, 683-706.
9. A. Salimi and A. A. Yousefi, *Polymer Testing*, 2003, 22, 699-704.
10. I. N. Bhatti, M. Banerjee and I. N. Bhatti, *IOSR-JAP*, 2013, 4, 42-47.
11. D.-W. Kim, G.-G. Lee and B.-E. Park, *Journal of the Korean Physical Society*, 2007, 51, 719-722.
12. H. D. Espinosa, R. A. Bernal and M. Minary☐Jolandan, *Advanced Materials*, 2012, 24, 4656-4675.
13. G. Ico, A. Showalter, W. Bosze, S. C. Gott, B. S. Kim, M. P. Rao, N. V. Myung and J. Nam, *Journal of Materials Chemistry A*, 2016, 4, 2293-2304.
14. D. Mandal, S. Yoon and K. J. Kim, *Macromolecular rapid communications*, 2011, 32, 831-837.
15. X. Liu, S. Xu, X. Kuang, D. Tan and X. Wang, *RSC Advances*, 2016, 6, 109061-109066.
16. C. Wan and C. R. Bowen, *Journal of Materials Chemistry A*, 2017, 5, 3091-3128.
17. M. Richard-Lacroix and C. Pellerin, *Macromolecules*, 2015, 48, 4511-4519.
18. U. Stachewicz, R. J. Bailey, W. Wang and A. H. Barber, *Polymer*, 2012, 53, 5132-5137.
19. J.-Y. Ke, H.-J. Chu, Y.-H. Hsu and C.-K. Lee.
20. U. Yaqoob, A. S. M. I. Uddin and G.-S. Chung, *Applied Surface Science*, 2017, 405, 420-426.
21. L. Persano, C. Dagdeviren, Y. Su, Y. Zhang, S. Girardo, D. Pisignano, Y. Huang and J. A. Rogers, *Nature communications*, 2013, 4, 1633.
22. S. R. Anton, A. Erturk and D. J. Inman, *IEEE transactions on ultrasonics, ferroelectrics, and frequency control*, 2012, 59, 1085-1092.
23. B. Yang, C. Lee, W. L. Kee and S. P. Lim, *Journal of Micro/Nanolithography, MEMS, and MOEMS*, 2010, 9, 023002-023002.
24. A. Koka and H. A. Sodano, *Advanced Energy Materials*, 2014, 4.
25. K.-I. Park, S. Xu, Y. Liu, G.-T. Hwang, S.-J. L. Kang, Z. L. Wang and K. J. Lee, *Nano letters*, 2010, 10, 4939-4943.
26. Y.-B. Park, J. L. Ruglovsky and H. A. Atwater, *Applied Physics Letters*, 2004, 85, 455-457.
27. Y. F. Hou, W. L. Li, T. D. Zhang, W. Wang, W. P. Cao, X. L. Liu and W. D. Fei, *Physical Chemistry Chemical Physics*, 2015, 17, 11593-11597.
28. M. V. Kakade, S. Givens, K. Gardner, K. H. Lee, D. B. Chase and J. F. Rabolt, *Journal of the American Chemical Society*, 2007, 129, 2777-2782.

29. J. Ma, Q. Zhang, A. Mayo, Z. Ni, H. Yi, Y. Chen, R. Mu, L. M. Bellan and D. Li, *Nanoscale*, 2015, 7, 16899-16908.
30. G. S. Y. Yeh, R. Hosemann, J. Loboda-Čačković and H. Čačković, *Polymer*, 1976, 17, 309-318.
31. S.-Y. Min, Y.-H. Kim, C. Wolf and T.-W. Lee, *ACS applied materials & interfaces*, 2015, 7, 18909-18914.
32. R. Agrawal and H. D. Espinosa, *Nano letters*, 2011, 11, 786-790.
33. J. Wang, Z. Huang, H. Duan, S. Yu, X. Feng, G. Wang, W. Zhang and T. Wang, *Acta Mechanica Solida Sinica*, 2011, 24, 52-82.
34. P. Zubko, G. Catalan and A. K. Tagantsev, *Annual Review of Materials Research*, 2013, 43, 387-421.
35. M. S. Majdoub, P. Sharma and T. Cagin, *Physical Review B*, 2008, 77, 125424.
36. F. Wang, J. B. Wang, X. L. Zhong, B. Li, Y. Zhang, C. J. Lu, W. N. Ye and Y. C. Zhou, *EPL (Europhysics Letters)*, 2013, 103, 37002.
37. S. S. Nonnenmann, O. D. Leaffer, E. M. Gallo, M. T. Coster and J. E. Spanier, *Nano letters*, 2010, 10, 542-546.
38. S. Dai, M. Gharbi, P. Sharma and H. S. Park, *Journal of Applied Physics*, 2011, 110, 104305.
39. J. Zhang, C. Wang and S. Adhikari, *Journal of Physics D: Applied Physics*, 2012, 45, 285301.
40. S. Baskaran, X. He, Q. Chen and J. Y. Fu, *Applied Physics Letters*, 2011, 98, 2901.
41. M. Richard-Lacroix and C. Pellerin, *Macromolecules*, 2014, 48, 37-42.
42. N. E. Zander, K. E. Strawhecker, J. A. Orlicki, A. M. Rawlett and T. P. Beebe Jr, *The Journal of Physical Chemistry B*, 2011, 115, 12441-12447.

Figure Captions

Figure 1. Morphology and piezoelectric properties of P(VDF-TrFE) nanofibers with various fiber diameters. (a – d) Scanning electron microscopy (SEM) images of electrospun P(VDF-TrFE) nanofibers with an average fiber diameter of 90 nm (a and c) and 30 nm (b and d) before (a and b) or after (c and d) a thermal treatment at 90 °C for 24 hours (scale bar = 1 μm). (e, f) Piezoelectric responses from individual P(VDF-TrFE) nanofibers before (e) and after (f) the thermal treatment, determined by piezoresponse force microscopy (PFM). (g) Piezoelectric coefficient (d_{33}) as a function of fiber diameter for as-spun or thermo-treated P(VDF-TrFE) nanofibers (n=5).

Figure 2. Piezoelectric performance and durability of P(VDF-TrFE) nanofibers. (a and b) Applied strain-dependent electric outputs ((a) peak-to-peak voltage and (b) peak-to-peak power) of P(VDF-TrFE) nanofibrous mats. (c) Open circuit voltage responses before and after 10,000 cycles of straining at 2 Hz. (d) Wearable P(VDF-TrFE) nanofibrous mat piezoelectric armband (i) powering a different maximum number of blue LEDs (off (ii-iii) and on (iv-v)) with either non-treated 90 nm diameter fibers (ii & iv) or thermo-treated 30 nm diameter fibers (iii & v).

Figure 3. Fiber size- and thermal treatment-dependent changes in electroactive phase content and their correlation to the piezoelectric coefficient, d_{33}. (a) FTIR spectra of electrospun P(VDF-TrFE) mats composed of nanofibers with an average diameter of 30 or 90 nm with or without a thermal treatment at 90 °C for 24 hours were used to quantify electroactive phase content in (b). (c) XRD spectra of electrospun P(VDF-TrFE) mats composed of nanofibers with an average diameter of 30 or 90 nm with or without the thermal treatment at 90 °C were used to calculate degree of crystallinity in (d). (e) The overall electroactive phase content calculated from (b) and (d). (f) Correlation between d_{33} and overall electroactive phase of P(VDF-TrFE) nanofibers.

Figure 4. Phase angle distribution of P(VDF-TrFE) nanofibers with an average diameter of 90 or 30 nm with or without the thermal treatment at 90 °C. (a) As-spun 90 nm diameter fibers showing a wider phase angle distribution centered approximately around 15.3° compared to (b) the thermo-treated 90 nm nanofibers,

determined from the corresponding representative PFM phase image shown above the histogram. (c) The decrease in fiber diameter from 90 nm to 30 nm narrowed the phase angle distribution and (d) was further narrowed by the thermal treatment, yielding a tighter distribution around 2.7°. n = 3000 (1000 measurement points, 3 independent fibers)

Figure 5. The effects of nanofibrous structure on the piezoelectric properties of P(VDF-TrFE). (a) Destruction of nanofibrous morphology, from P(VDF-TrFE) nanofibers with an average diameter of 30 nm, after the thermal treatment at 135 °C, examined by SEM (scale bar = 1μm). (b) Thermal treatment-dependent electroactive phase content of P(VDF-TrFE) nanofiber mats with an average fiber diameter of 30 nm. (c) PFM comparison of an individual 30 nm fiber and a melted film after the thermal treatment of a mat composed of multiple 30 nm fibers both at 135 °C. (d) Peak-to-peak voltage comparison of 30 nm nanofiber mats at 23, 90, and 135 °C.

Figure 6. Fiber diameter dependent strain gradient. (a) Measured Young's modulus of P(VDF-TrFE) nanofibers as a function of fiber diameter and fitted with a rule of mixture equation to calculate the sheath thickness, and the core/sheath modulus of the nanofibers. (b) The cross-sectional strain distribution within the fiber of 30 nm or 90 nm diameter under a fixed -15% mechanical strain, simulated by COMSOL. (c) Strain gradient within the fiber of 30 nm or 90 nm diameter as a function of cross sectional length (perpendicular to the length of the nanofiber).
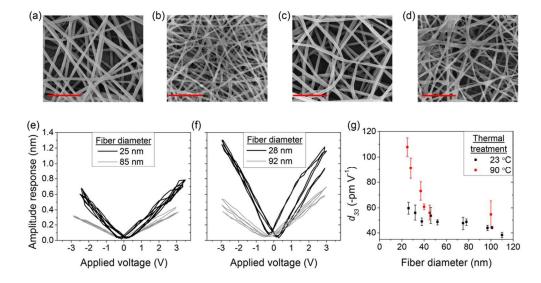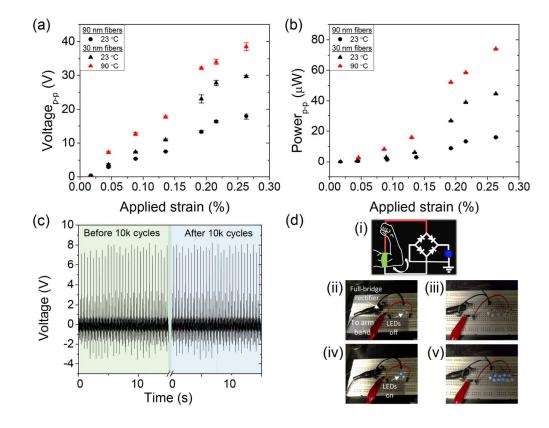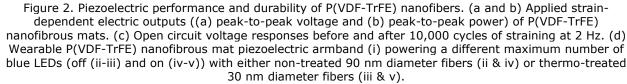
Figure 1. Morphology and piezoelectric properties of P(VDF-TrFE) nanofibers with various fiber diameters. (a – d) Scanning electron microscopy (SEM) images of electrospun P(VDF-TrFE) nanofibers with an average fiber diameter of 90 nm (a and c) and 30 nm (b and d) before (a and b) or after (c and d) a thermal treatment at 90 °C for 24 hours (scale bar = 1 μm). (e, f) Piezoelectric responses from individual P(VDF-TrFE) nanofibers before (e) and after (f) the thermal treatment, determined by piezoresponse force microscopy (PFM). (g) Piezoelectric coefficient (d33) as a function of fiber diameter for as-spun or thermo-treated P(VDF-TrFE) nanofibers (n = 5).

89x46mm (300 x 300 DPI)

Figure 2. Piezoelectric performance and durability of P(VDF-TrFE) nanofibers. (a and b) Applied strain-dependent electric outputs ((a) peak-to-peak voltage and (b) peak-to-peak power) of P(VDF-TrFE) nanofibrous mats. (c) Open circuit voltage responses before and after 10,000 cycles of straining at 2 Hz. (d) Wearable P(VDF-TrFE) nanofibrous mat piezoelectric armband (i) powering a different maximum number of blue LEDs (off (ii-iii) and on (iv-v)) with either non-treated 90 nm diameter fibers (ii & iv) or thermo-treated 30 nm diameter fibers (iii & v).

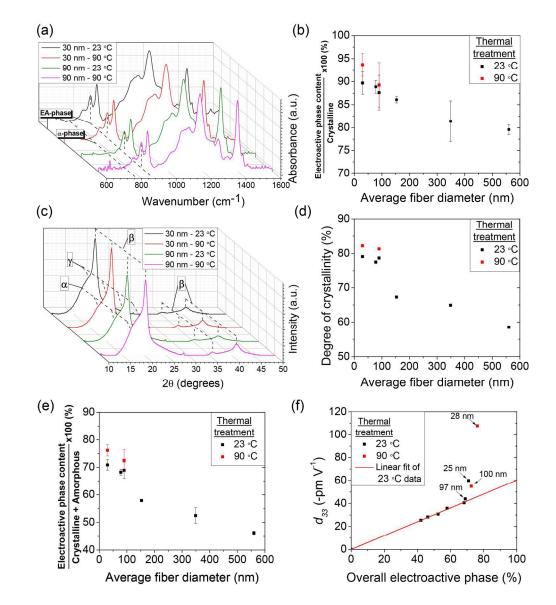134x106mm (300 x 300 DPI)

Nanoscale

Figure 3. Fiber size- and thermal treatment-dependent changes in electroactive phase content and their correlation to the piezoelectric coefficient, d33. (a) FTIR spectra of electrospun P(VDF-TrFE) mats composed of nanofibers with an average diameter of 30 or 90 nm with or without a thermal treatment at 90 °C for 24 hours were used to quantify electroactive phase content in (b). (c) XRD spectra of electrospun P(VDF-TrFE) mats composed of nanofibers with an average diameter of 30 or 90 nm with or without the thermal treatment at 90 °C were used to calculate degree of crystallinity in (d). (e) The overall electroactive phase content calculated from (b) and (d). (f) Correlation between d33 and overall electroactive phase of P(VDF-TrFE) nanofibers.
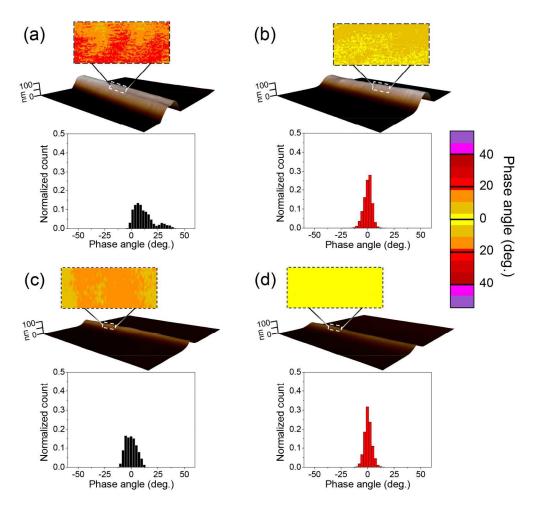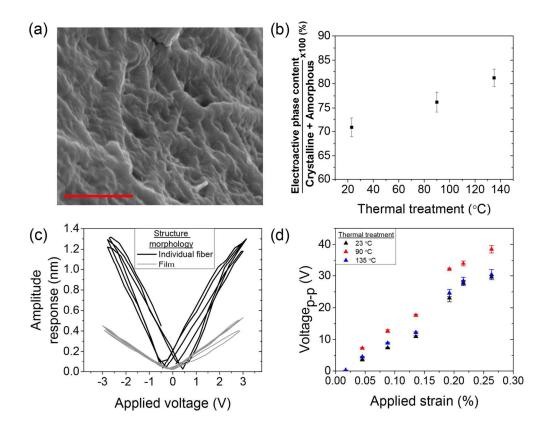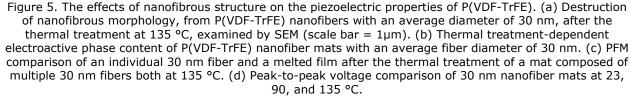
194x221mm (300 x 300 DPI)

Figure 4. Phase angle distribution of P(VDF-TrFE) nanofibers with an average diameter of 90 or 30 nm with or without the thermal treatment at 90 °C. (a) As-spun 90 nm diameter fibers showing a wider phase angle distribution centered approximately around 15.3° compared to (b) the thermo-treated 90 nm nanofibers, determined from the corresponding representative PFM phase image shown above the histogram. (c) The decrease in fiber diameter from 90 nm to 30 nm narrowed the phase angle distribution and (d) was further narrowed by the thermal treatment, yielding a tighter distribution around 2.7°. (n = 3000 (1000 measurement points, 3 independent fibers)).

162x152mm (300 x 300 DPI)

Figure 5. The effects of nanofibrous structure on the piezoelectric properties of P(VDF-TrFE). (a) Destruction of nanofibrous morphology, from P(VDF-TrFE) nanofibers with an average diameter of 30 nm, after the thermal treatment at 135 °C, examined by SEM (scale bar = 1μm). (b) Thermal treatment-dependent electroactive phase content of P(VDF-TrFE) nanofiber mats with an average fiber diameter of 30 nm. (c) PFM comparison of an individual 30 nm fiber and a melted film after the thermal treatment of a mat composed of multiple 30 nm fibers both at 135 °C. (d) Peak-to-peak voltage comparison of 30 nm nanofiber mats at 23, 90, and 135 °C.
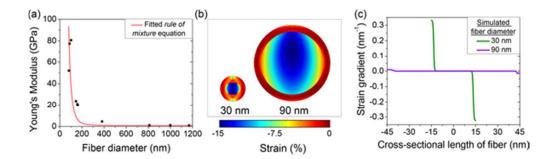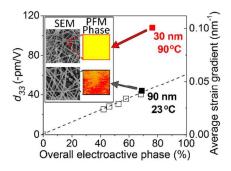
135x107mm (300 x 300 DPI)

Figure 6. Fiber diameter dependent strain gradient. (a) Measured Young's modulus of P(VDF-TrFE) nanofibers as a function of fiber diameter and fitted with a rule of mixture equation to calculate the sheath thickness, and the core/sheath modulus of the nanofibers. (b) The cross-sectional strain distribution within the fiber of 30 nm or 90 nm diameter under a fixed -15% mechanical strain, simulated by COMSOL. (c) Strain gradient within the fiber of 30 nm or 90 nm diameter as a function of cross sectional length (perpendicular to the length of the nanofiber).

49x14mm (300 x 300 DPI)

P(VDF-TrFE) nanofibers show exceptional piezoelectricity through the synergistic relationship between dimensional reduction to the 30 nm scale and thermal treatment.